CHEMISTRY
A EUROPEAN JOURNAL

ChemPubSoc
Europe

DOI: 10.1002/chem.201200919

Controlled Self-Assembly by Mono-*p*-sulfonatocalix[*n*]arenes and Bis-*p*-sulfonatocalix[*n*]arenes

Kui Wang, Dong-Sheng Guo, and Yu Liu*[a]

Abstract: The complexation-induced critical aggregation concentrations of 1-pyrenemethylaminium by mono-*p*-sulfonatocalix[*n*]arenes and bis-*p*-sulfonatocalix[*n*]arenes ($n=4$, 5) were systemically measured by fluorescence spectroscopy. In all cases, the complexation-induced critical aggregation concentration decreases by about 3 times upon addition of *p*-sulfonatocalix[*n*]arenes. However, the optimal molar ratios for the aggregation of 1-pyrenemethylaminium by mono-*p*-sulfonatocalix[*n*]arenes and bis-*p*-sulfonatocalix[*n*]arenes are distinctly different: For mono-*p*-sulfonatocalix[*n*]arenes, the optimum mixing ratio for the aggregation of 1-pyrenemethylaminium is 1:4 mono-*p*-sulfonatocalix[*n*]arenes/1-pyrenemethylaminium, whereas only 2.5 molecules of 1-pyrenemethylaminium can be bound by one cavity of bis-*p*-sulfonatocalix[*n*]arenes. The intermolecular complexation of mono-*p*-sulfonatocalix[*n*]arenes and bis-*p*-sulfonatocalix[*n*]arenes with 1-pyrenemethylaminium led to the formation of two distinctly different nanoarchitectures, which were shown to be nanoscale vesicle and rod aggregates, respectively, by using dynamic laser scattering, TEM, and SEM. This behavior is also different from the fiber-like aggregates with lengths of several micrometers that were formed by 1-pyrenemethylaminium itself above its critical aggregation concentration. Furthermore, the obtained nanoaggregates exhibit benign water solubility, self-labeled fluorescence, and, more importantly, temperature responsiveness.

Keywords: aggregation · calixarenes · host–guest systems · pyrenes · self-assembly

Introduction

Molecular self-assembly is an attractive and powerful strategy for fabricating nanoarchitectures. Self-assembly processes are ubiquitous in chemistry, materials science, and biology.[1] The morphology of the assembly can potentially be precisely manipulated by the rational design and modification of the building blocks at the molecular level.[2] Nature has provided a large number of examples that perfectly elucidate this concept, such as stem cells and membrane structures in the endoplasmic reticulum.[2a,3] In this context, the construction of controlled nanoscale structures and materials with well-defined shapes and dimensions from molecular components is of great interest.[4]

Benefiting from the upper-rim sulfonated groups, *p*-sulfonatocalix[*n*]arenes (SC*n*As) are one of the most-important calixarene derivatives because they display especially strong binding ability and high molecular selectivity towards the target guest compounds in water.[5] "Moreover, having the intrinsic advantages of calixarenes, the conformations and rigid degrees of SC*n*As can be precisely manipulated by modifying their lower rims.[5a,6] Consequently, SC*n*As are one class of potential macrocyclic compounds for constructing controlled supramolecular assemblies by host–guest complexation in aqueous solution. However, there has been little research in this area,[7] especially on the comparison of mono-*p*-sulfonatocalix[*n*]arenes (*mono*-SC*n*As) and bis-*p*-sulfonatocalix[*n*]arenes (*bis*-SC*n*As). In a previous work, we reported the construction of a supramolecular binary vesicle upon complexation of mono-*p*-sulfonatocalix[5]arene (*mono*-SC5A) with 1-pyrenemethylaminium (PMA) guests.[7c] Following that work, herein, we found that the complexation of mono-*p*-sulfonatocalix[4]arene (*mono*-SC4A) with PMA can also self-assemble into nanoscale vesicle aggregates. We intended to cross-link the resulting vesicles together to construct supramolecular hydrogels by replacing *mono*-SC*n*As with *bis*-SC*n*As ($n=4$, 5). Unexpectedly, the aggregation behavior of PMA with *bis*-SC*n*As was dramatically different, with the fabrication of 1D linear nanorod aggregates. This behavior is also distinguishable from the fiber-like aggregates with lengths of several micrometers that were formed by PMA itself above its critical aggregation concentration (CAC). Notably, a minimum of two interacting sites is normally required to form a 1D linear morphology from two complementary monomers.[7b] However, PMA, one of the two components used herein to construct nanorod structures, only has one interacting site. Herein, we develop a new design idea for utilizing host-sta-

[a] K. Wang, Dr. D.-S. Guo, Prof. Dr. Y. Liu
Department of Chemistry
State Key Laboratory of Elemento-Organic Chemistry
Nankai University, Tianjin 300071 (P.R. China)
Fax: (+86) 22-2350-3625
E-mail: yuliu@nankai.edu.cn

Supporting information for this article is available on the WWW under http://dx.doi.org/10.1002/chem.201200919.

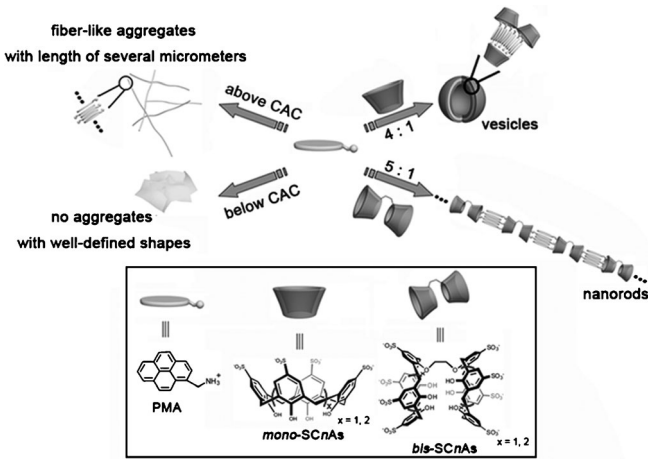

Scheme 1. Three distinctly different architectures of PMA aggregates in the absence and presence of *mono*-SC*n*As or *bis*-SC*n*As.

bilized guest aggregation in fabricating 1D supramolecular linear assemblies by host–guest complexation (Scheme 1).

Results and Discussion

The CAC values of PMA in the absence and presence of *mono*-SC5A were reported in our previous work and we found that the value for free PMA was 0.27 mM, whereas, upon addition of *mono*-SC5A, that value would decrease by about 3 times.[7c] Herein, to compare the complexation-induced CAC of PMA by *mono*-SC*n*As and *bis*-SC*n*As, the CAC values of PMA in the presence of different concentrations of *mono*-SC4A, bis-*p*-sulfonatocalix[4]arene (*bis*-SC4A), and bis-*p*-sulfonatocalix[5]arene (*bis*-SC5A) were systemically measured by monitoring the polarity of the surrounding medium of pyrene (dependence of the fluorescence-intensity ratio (I_b/I_a) of PMA on its concentration).[8] The results show that the complexation-induced CAC of PMA by *mono*-SC*n*As and *bis*-SC*n*As are similar (see the Supporting Information, Figures S1–S3): on average, 0.09 mM for *mono*-SC4A (0.10 mM at 0.02 mM *mono*-SC4A, 0.06 mM at 0.04 mM *mono*-SC4A, and 0.10 mM at 0.06 mM *mono*-SC4A), 0.07 mM for *bis*-SC4A (0.06 mM at 0.02 mM *bis*-SC4A, 0.08 mM at 0.04 mM *bis*-SC4A, and 0.06 mM at 0.06 mM *bis*-SC4A), and 0.10 mM for *bis*-SC5A (0.10 mM at 0.02 mM *bis*-SC5A, 0.10 mM at 0.04 mM *bis*-SC5A, and 0.09 mM at 0.06 mM *bis*-SC5A); all of these values decrease by about 3 times upon the addition of SC*n*As. Notably, the SC*n*As themselves have no tendency to self-aggregate in aqueous solution.[9]

Although the complexation-induced CAC of PMA by *mono*-SC*n*As and *bis*-SC*n*As are similar, the optimal molar ratios of *mono*-SC*n*As and *bis*-SC*n*As that lead to PMA aggregation are distinctly different. The values of I_b/I_a and I_{483} (the excimer emission of pyrene) as a function of the concentration of the SC*n*As (at a fixed PMA concentration of 0.20 mM) undergo a pronounced increase and then a decrease upon a gradual addition of SC*n*As (see the Supporting Information, Figures S4–S6). In the left-hand portion of the inflexion, SC*n*As and PMA form a higher-order complex with a tendency toward self-aggregation, whereas in the right-hand portion of inflexion, excess SC*n*As lead to the formation of a simple inclusion complex, which is accompanied by the disassembly of the aggregates. For *mono*-SC4A, the inflexion appears at a *mono*-SC4A/PMA molar ratio of 0.25 (see the Supporting Information, Figure S4), thereby indicating that the optimal mixing ratio for PMA aggregation is 1:4 *mono*-SC4A/PMA, which is the same as that for the *mono*-SC5A+PMA system. However, for *bis*-SC*n*As, that ratio is 1:5 *bis*-SC*n*As/PMA (see the Supporting Information, Figures S5 and S6), thus indicating that only 2.5 molecules of PMA can be bound with one cavity of *bis*-SC*n*As. As can be seen from the energy-minimized structures of *mono*-SC*n*As and *bis*-SC*n*As, which were obtained by a molecular modeling study (Figure 1; also see the Supporting Information, Figure S7), the cavity of the *bis*-SC*n*As becomes pinched compared with that of the *mono*-SC*n*As upon *mono*-bridging linkage at its lower rim; as a result, less

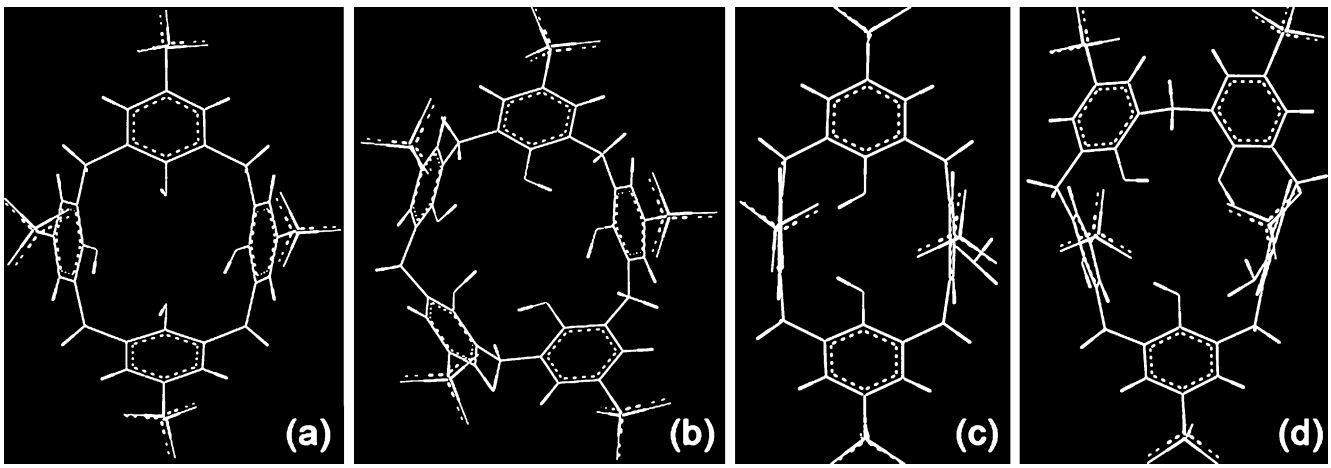

Figure 1. Energy-minimized structures of: a) *mono*-SC4A, b) *mono*-SC5A, c) one cavity of *bis*-SC4A, and d) one cavity of *bis*-SC5A, which were obtained by molecular modeling; the geometries were optimized by the molecular mechanics method with a Dreiding force field.

PMA molecules can be bound. One reasonable explanation for the pinched cavity of the *bis*-SC*n*As is that the framework of the *bis*-SC*n*As becomes more rigid compared with that of the *mono*-SC*n*As because the *mono*-bridging linkage of two cavities at the lower rim restrains the mobility of the aromatic rings that are linked by the spacer. This explanation is supported by the experimental results with 5,11,17,23-tetrasulfonato-25,26,27,28-tetrakis(ethyl)-calix[4]-arene (*mono*-SC4A-Et). As can be seen from the energy-minimized structure of *mono*-SC4A-Et (see the Supporting Information, Figure S8a), the cavity of *mono*-SC4A-Et becomes much-more pinched compared with that of the *bis*-SC*n*As; as a result, fewer PMA molecules can be bound by the cavity of *mono*-SC4A-Et (for *mono*-SC4A-Et, the optimum mixing ratio for PMA aggregation is 1:1 *mono*-SC4A-Et/PMA; see the Supporting Information, Figure S9). Reasonably, the steric hindrance from the four ethyl groups of *mono*-SC4A-Et at the lower rim is much larger than that from the *mono*-bridging linkage of the *bis*-SC*n*As; hence, the framework of *mono*-SC4A-Et is more rigid compared with that of the *bis*-SC*n*As. The much-more-rigid framework of *mono*-SC4A-Et was also confirmed by its ^{1}H NMR spectrum in D_2O (see the Supporting Information, Figure S8b). The bridging methylene protons of *mono*-SC4A show a single peak, thereby indicating that the *mono*-SC*n*As have a flexible conformation in aqueous solution. However, the bridging methylene protons of *mono*-SC4A-Et show two peaks in its ^{1}H NMR spectrum, thus revealing that the framework of *mono*-SC4A-Et is much-more rigid because the steric hindrance from the four ethyl groups of *mono*-SC4A-Et at the lower rim restrains a random flipping motion of the aromatic rings, which is also in accordance with our previously reported results on 5,11,17,23-tetrasulfonato-25,26,27,28-tetrakis(*n*-butyl)-calix[4]arene.[6]

We compared the UV/Vis absorption and fluorescence emission spectra of PMA in the presence of SC*n*As and 4-phenolsulfonic sodium, the building subunit of SC*n*As, as control experiments (Figure 2). Upon the addition of SC*n*As, a broad absorption that corresponds to the characteristic absorption of the charge-transfer complex appears between 400 and 550 nm;[2a] moreover, the monomer emission diminishes, whereas the excimer emission emerges, accompanied by an evolution from blue to green fluorescence (see the Supporting Information, Figure S10a), thus indicating the aggregation of pyrene segments. However, the addition of excess 4-phenolsulfonic sodium does not cause any appreciable change in both the absorption and emission spectra of PMA, thereby undoubtedly indicating that the host–guest complexation of SC*n*As is the crucial factor that leads to PMA aggregation, in which the electrostatic interactions between negatively charged sulfonated groups and the positively charged amino groups reinforces the stability of the complex. On the other hand, a solution of SC*n*As+PMA exhibits a clear Tyndall effect, thus indicating the existence of abundant nanoparticles, whereas this effect is not observed for the solution of free PMA (see the Supporting Information, Figure S10b). This phenomenon reveals that

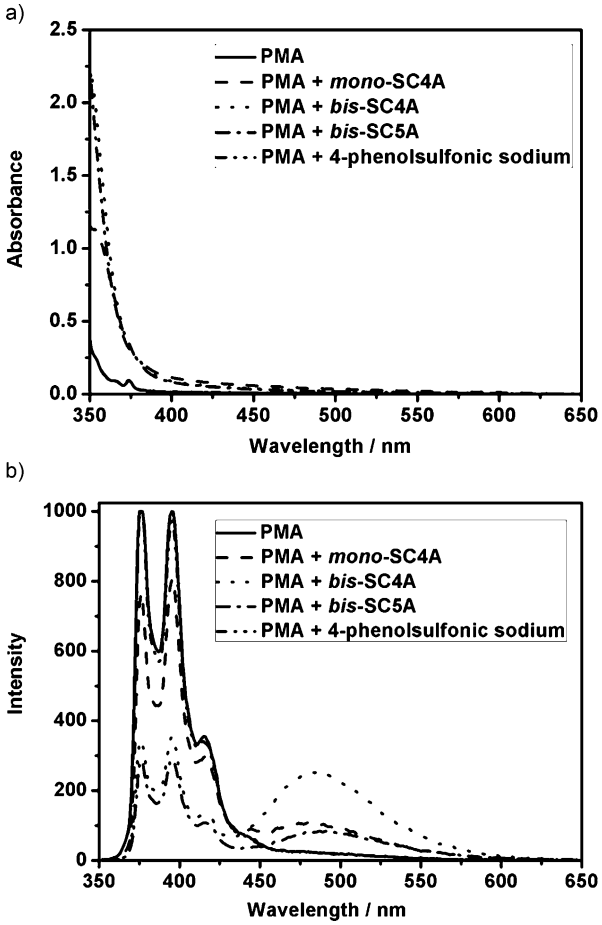

Figure 2. a) UV/Vis absorption, and b) fluorescence emission spectra of PMA, PMA+*mono*-SC4A, PMA+*bis*-SC4A, PMA+*bis*-SC5A, and PMA+4-phenolsulfonic sodium at 25 °C in water. λ_{ex} = 335.0 nm, bandwidth (ex): 2.5 nm, bandwidth (em): 5.0 nm; [PMA] = 0.20 mM, [*mono*-SC4A] = 0.05 mM, [*bis*-SC4A] = 0.04 mM, [*bis*-SC5A] = 0.04 mM, [4-phenolsulfonic sodium] = 0.40 mM.

the free PMA blocks cannot form nanoscale aggregates themselves at 0.20 mM, although they have a stacking capability above their CAC (1.00 mM) with respect to the fluorescence emission (see the Supporting Information, Figure S10c).

Furthermore, dynamic laser scattering (DLS), TEM, and SEM were used to identify the size and morphology of the self-assembled SC*n*As+PMA aggregates. No signal was observed for free PMA at 0.20 mM in the DLS measurements and no aggregates with well-defined shapes were found in the TEM and SEM images (see the Supporting Information, Figure S11). Upon addition of *mono*-SC4A, both the DLS results (Figure 3) and the TEM and SEM images (Figure 4) confirm that *mono*-SC4A+PMA can also self-assemble into nanoscale vesicle aggregates, as in the case of *mono*-SC5A+PMA. The DLS results show that the *mono*-SC4A+PMA complex forms spectacular aggregates with a size distribution of 22–247 nm, and gives an average diameter of 166 nm. The diameters of the aggregates exceed their corresponding extended molecular length, thereby sug-

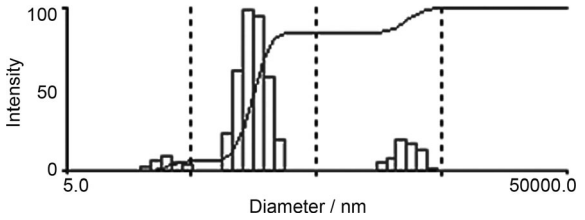

Figure 3. DLS data of the PMA+*mono*-SC4A aggregates; [PMA] = 0.20 mM, [*mono*-SC4A] = 0.05 mM.

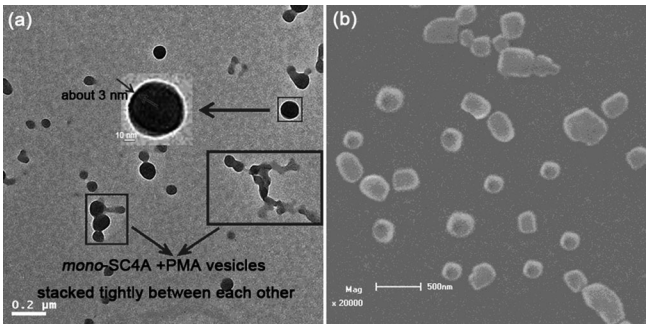

Figure 4. a) TEM (scale bar: 0.2 μm), and b) SEM (scale bar: 500 nm) images of the PMA+*mono*-SC4A aggregates; [PMA] = 0.20 mM, [*mono*-SC4A] = 0.05 mM.

gesting that these aggregates are vesicular entities than simple micelles.[10] Further evidence for the formation of vesicles is provided by the TEM images, which show the hollow spherical morphology, thus convincingly indicating the vesicular structure (Figure 4a). Moreover, from the distinguishable dark periphery and the light central parts in the TEM images, we obtained a thickness of the bilayer membrane of about 3 nm, which is in the same order of magnitude as the sum of one PMA length (7 Å)[11] and two *mono*-SC4A heights (14 Å),[12] thus indicating that the vesicle is unilamellar. Such spheres are also found in the SEM images (Figure 4b). Unlike the *mono*-SC5A+PMA vesicles,[7c] the *mono*-SC4A+PMA vesicles stack tightly between each other because *mono*-SC4A has a stronger stacking ability than *mono*-SC5A owing to its much-more-three-dimensional conformation,[12–14] which is also in accordance with the larger size distribution from 1612–4116 nm in the DLS results of *mono*-SC4A+PMA.

Surprisingly, the aggregation behavior of PMA with the *bis*-SC*n*As is dramatically different to that with the *mono*-SC*n*As. DLS results show that the *bis*-SC*n*As+PMA aggregates have a similar average diameter to the *mono*-SC*n*As+PMA aggregates: 194 nm for *bis*-SC4A+PMA and 174 nm for *bis*-SC5A+PMA (Figure 5). TEM images of the *bis*-SC*n*As+PMA aggregates clearly show 1D linear nanorods on the substrates (Figure 6). The width of the nanorods is about 1 nm, which is almost the same as the height of the SC*n*As. Such rods are also found in the SEM images (see the Supporting Information, Figure S12). For the same reason as the *mono*-SC*n*As, the *bis*-SC4A+PMA nanorod aggregates stack tightly between each other in the TEM

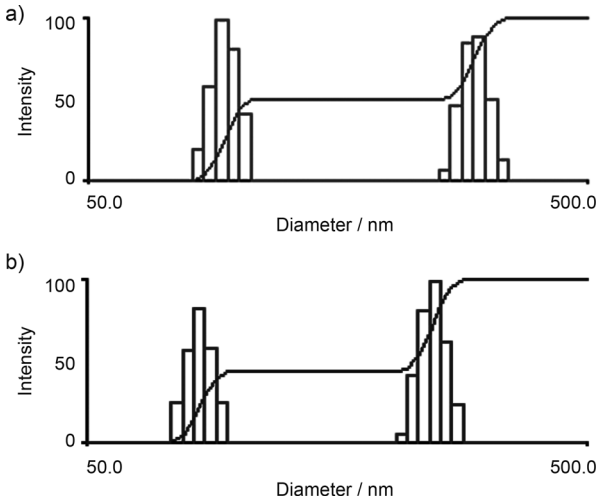

Figure 5. DLS data of the: a) PMA+*bis*-SC4A, and b) PMA+*bis*-SC5A aggregates; [PMA] = 0.20 mM, [*bis*-SC4A] = 0.04 mM, [*bis*-SC5A] = 0.04 mM.

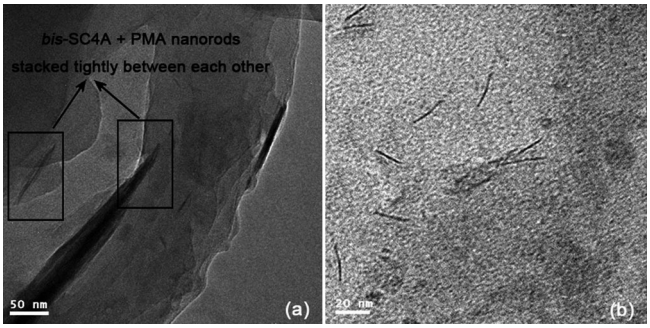

Figure 6. TEM images of the: a) PMA+*bis*-SC4A, and b) PMA+*bis*-SC5A aggregates; [PMA] = 0.20 mM, [*bis*-SC4A] = 0.04 mM, [*bis*-SC5A] = 0.04 mM.

images. We also wanted to compare the changes in the ^{1}H NMR chemical shifts of PMA after the addition of SC*n*As to deduce the binding modes between PMA and SC*n*As. Unfortunately, in the presence of SC*n*As, the ^{1}H NMR signals of PMA are significantly broadened and we could not recognize them clearly. However, this phenomenon confirmed the stacking of PMA that was induced by the complexation of the SC*n*As. On the other hand, SC*n*As have been well-known to bind the positively charged group of the guest by their upper-rim sulfonated cavities.[5] Combining all of these aforementioned results, we deduced a model for the formation of supramolecular nanorods (Scheme 1) in which the hydrophobic pyrene segments are packed together and the *bis*-SC*n*As and PMA are connected together through host–guest interactions. Notably, PMA only has one interacting site with the *bis*-SC*n*As; thus, a new design idea for utilizing host-stabilized–guest aggregation for fabricating 1D supramolecular linear assembly by host–guest complexation is proposed herein. As confirmed above, less PMA molecules can be bound with the cavity of *bis*-SC*n*As; as a result, the *bis*-SC*n*As+PMA complexes

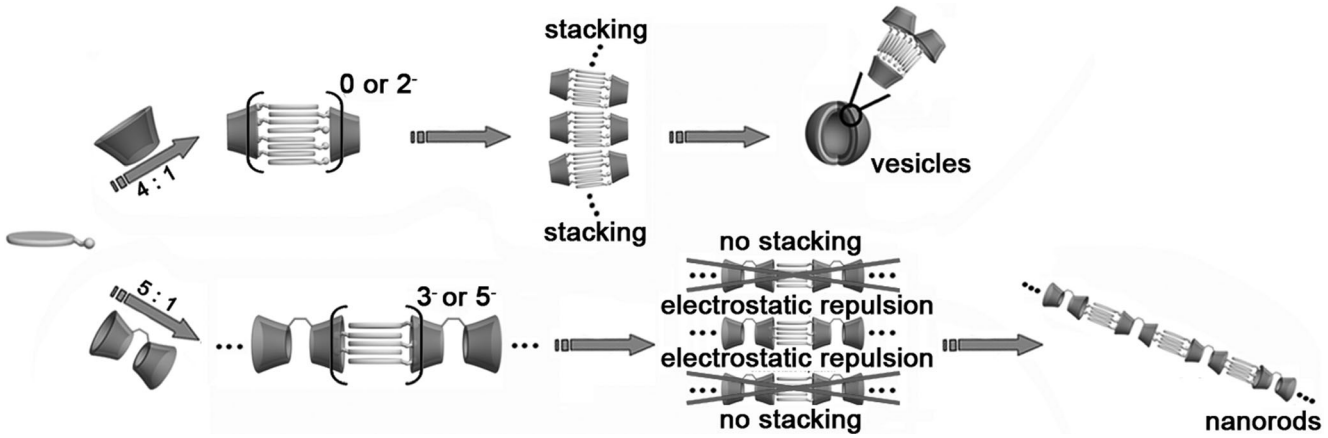

Scheme 2. An explanation for the distinctly different aggregation behavior of PMA in the presence of *mono*-SC*n*As and *bis*-SC*n*As.

have a stronger electrostatic repulsion between each other compared with the *mono*-SC*n*As+PMA complexes. In addition, the *bis*-SC*n*As have one more interacting site with PMA compared with the *mono*-SC*n*As. Both of these factors contribute to the distinctly different aggregation behaviors of PMA with the *bis*-SC*n*As (Scheme 2).

We also performed DLS measurements on the *bis*-SC*n*As+PMA aggregates with a PMA concentration above the CAC of free PMA; these results show that the average diameters become a little longer: 228 nm for *bis*-SC4A+PMA and 221 nm for *bis*-SC5A+PMA (Figure 7).

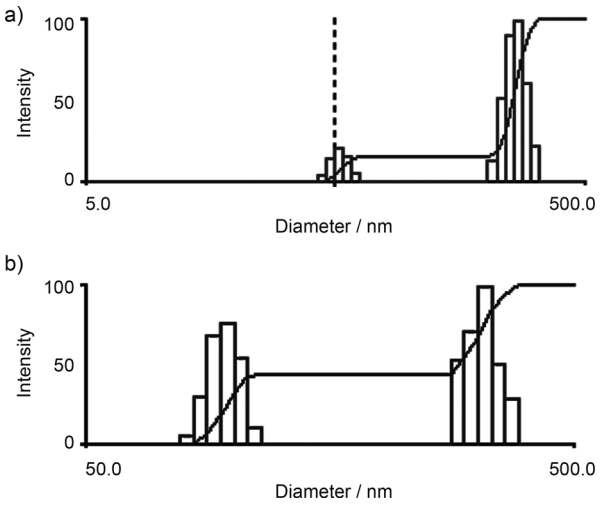

Figure 7. DLS data of the: a) PMA+*bis*-SC4A, and b) PMA+*bis*-SC5A aggregates above the CAC value of free PMA; [PMA] = 1.00 mM, [*bis*-SC4A] = 0.20 mM, [*bis*-SC5A] = 0.20 mM.

Both the TEM (Figure 8a, b) and SEM images (see the Supporting Information, Figure S13) show similar nanorods on the substrates (see above). Interestingly, PMA alone can form another distinctly different morphology above its CAC value, owing to π···π stacking along the vertical orientation of the PMA plane. A number of fiber-like aggregates with

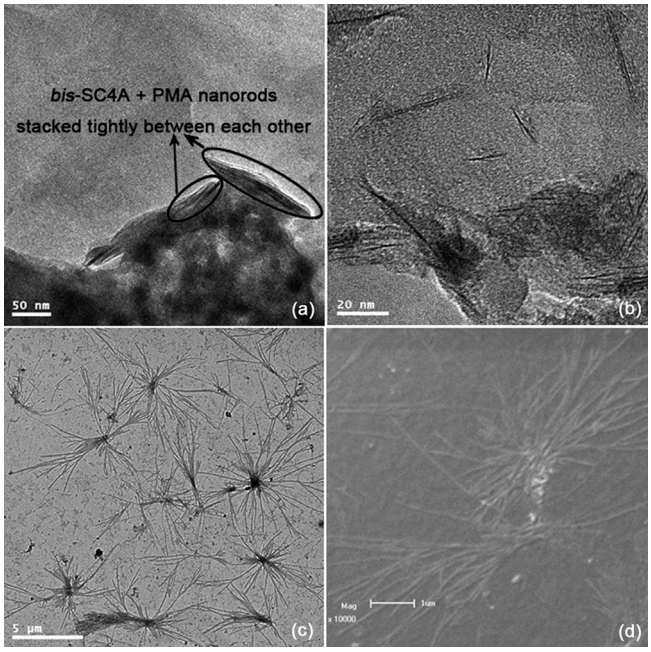

Figure 8. TEM images of the: a) PMA+*bis*-SC4A (scale bar: 50 nm), and b) PMA+*bis*-SC5A aggregates (scale bar: 20 nm) above the CAC value of free PMA; c) TEM (scale bar: 5 μm), and d) SEM (scale bar: 1 μm) images of PMA aggregates above its CAC value. [PMA] = 1.00 mM, [*bis*-SC4A] = 0.20 mM, [*bis*-SC5A] = 0.20 mM.

lengths of several micrometers are observed in both the TEM and SEM images (Figure 8c, d). Such fiber-like aggregates are also found in the optical-microscopy and fluorescence-microscopy images (see the Supporting Information, Figure S14).

Another significant point regarding this assembly study is concerned with their capability to respond to external stimuli because the ability to controllably switch an assembly on/off is a prerequisite for potential applications.[15] Similarly to the binary vesicles that are formed by the complexation of the *mono*-SC*n*As,[7c] the *bis*-SC*n*As+PMA nanorods are also satisfactorily sensitive to an external stimulus of tempera-

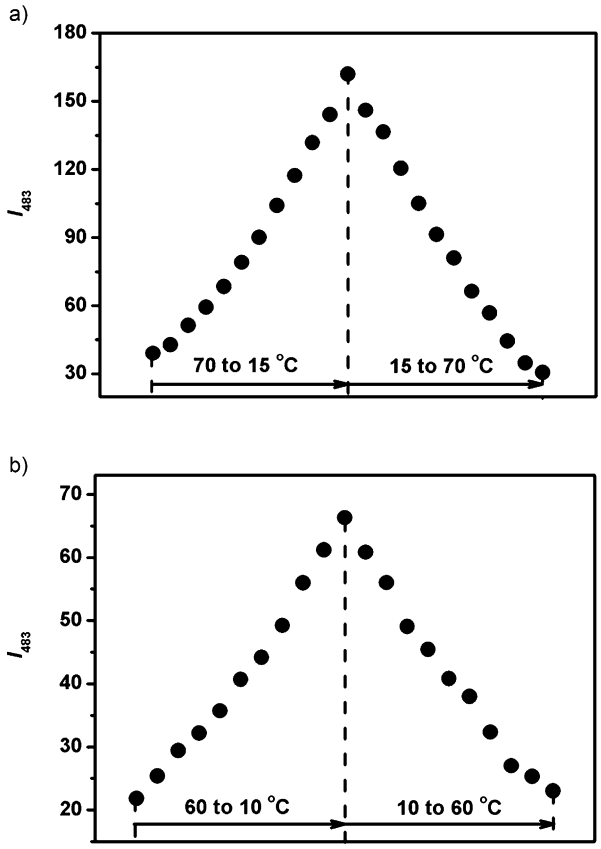

Figure 9. Dependence of the I_{483} value for the: a) PMA+*bis*-SC4A, and b) PMA+*bis*-SC5A aggregates on temperature; [PMA] = 0.20 mM, [*bis*-SC4A] = 0.04 mM, [*bis*-SC5A] = 0.04 mM.

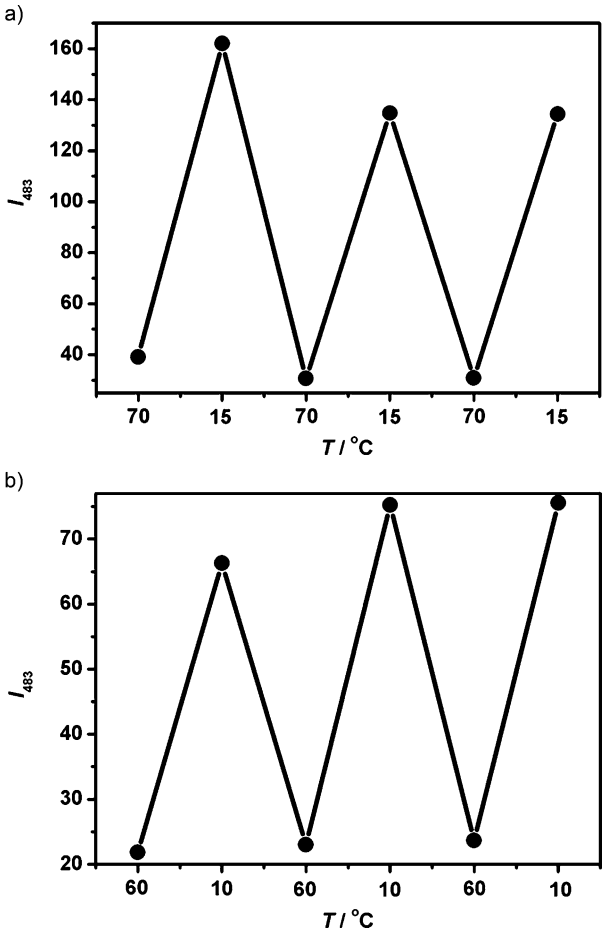

Figure 10. a) Changes in the I_{483} value for the PMA+*bis*-SC4A aggregates over several cycles of thermal equilibration at 15 and 70 °C. b) Changes in the I_{483} value for the PMA+*bis*-SC5A aggregates over several cycles of thermal equilibration at 10 and 60 °C; [PMA] = 0.20 mM, [*bis*-SC4A] = 0.04 mM, [*bis*-SC5A] = 0.04 mM.

ture. The excimer emission (I_{483}) of the *bis*-SC*n*As+PMA nanorods increases gradually with decreasing temperature and vice versa, which reflects the processes of assembly and disassembly, respectively (Figure 9). The left assembly curve is almost symmetrical with the right disassembly one; the same phenomenon was also observed for the I_b/I_a value (see the Supporting Information, Figure S15). Control fluorescence experiments were carried out with pyrene alone at 5 °C and 70 °C and no such variation occurred.[7d] This reversible assembly/disassembly process can be modulated repeatedly several times (Figure 10; also see the Supporting Information, Figure S16). The temperature response of the nanorod is acceptable for both the complexation of the SC*n*As with organic guests and the π···π stacking of aromatic pyrenes because they are enthalpy-driven processes that would be weakened upon warming.[5a,16] In other words, this temperature-responsive character also in part supports our model of the formation of the supramolecular nanorods (see above). The final disassembled products may be water-soluble *bis*-SC*n*As, PMA, and simple *bis*-SC*n*As+PMA inclusion complexes. Moreover, the assembly/disassembly process can be accomplished on the timescale of minutes or even-more rapidly with changing temperature, which endows these nanoaggregates with kinetic availability for further applications.

Conclusion

In conclusion, three distinctly different architectures of PMA aggregates in the absence and presence of *mono*-SC*n*As or *bis*-SC*n*As have been constructed. PMA and *mono*-SC*n*As can self-assemble into vesicle aggregates through host–guest complexation that benefit from the single flexible cavities of *mono*-SC*n*As. The aggregation behavior of PMA with *bis*-SC*n*As is dramatically different from that with *mono*-SC*n*As, which showed the fabrication of 1D linear nanorod aggregates. The reasons for the distinctly different aggregation behavior of PMA with *bis*-SC*n*As may be the distinguishable number and rigidity of their cavity compared with that of *mono*-SC*n*As. This behavior is also different from the fiber-like aggregates with lengths of several micrometers that were formed by PMA itself above its CAC owing to π···π stacking along the vertical orientation of the PMA plane. Furthermore, the obtained nanoaggregates exhibit benign water solubility, self-labeled fluorescence, and, more importantly, temperature responsiveness. This observation will allow us to rationally

design and construct a wide range of functional supramolecular nanoarchitectures and nanomaterials by carefully choosing the right combinations of molecular building blocks.

Experimental Section

Materials preparation: 1-Pyrenemethylaminium and 4-phenolsulfonic sodium were commercially available from Aldrich and Acros, respectively, and used without further purification. Mono-*p*-sulfonatocalix[4]arene,[17] mono-*p*-sulfonatocalix[5]arene,[18] bis-*p*-sulfonatocalix[4]arene,[7b] bis-*p*-sulfonatocalix[5]arene,[7a] and 5,11,17,23-tetrasulfonato-25,26,27,28-tetrakis(ethyl)-calix[4]arene[19] were synthesized and purified according to literature procedures; these compounds were characterized by ^{1}H NMR and ^{13}C NMR spectroscopy (D_2O) on a Varian 300 spectrometer and by elemental analysis on a Perkin–Elmer-2400C instrument.

UV/Vis absorption and fluorescence emission spectra: UV/Vis spectra were recorded in a quartz cell (light path 10 mm) on a Shimadzu UV-3600 spectrophotometer that was equipped with a PTC-348WI temperature controller. Steady-state fluorescence spectra were recorded in a conventional quartz cell (light path 10 mm) on a Varian Cary Eclipse that was equipped with a Varian Cary single-cell peltier accessory to control temperature.

DLS measurements: The sample solution for the DLS measurements was prepared by filtering the solution through a 450 nm Millipore filter into a clean scintillation vial. The samples were examined on a laser-light-scattering spectrometer (BI-200SM) that was equipped with a digital correlator (Turbo Corr.) at 532 nm and a scattering angle of 90°.

TEM and SEM experiments: TEM images were recorded on a Philips Tecnai G2 20S-TWIN microscope operating at an accelerating voltage of 200 keV. The sample for TEM measurements was prepared by dropping the solution onto a copper grid. The grid was then air-dried. SEM images were recorded on a Hitachi S-3500N SEM. The sample for SEM measurements was prepared by dropping the solution onto a coverslip, followed by evaporating the liquid in air.

Optical and fluorescence microscopy experiments: One drop of the sample solution was dropped onto a glass slip and the optical and fluorescence microscopic images were performed on an OLYMPUS BX51 fluorescence microscope (Anaheim, USA) with a 100 W DC mercury lamp for excitation and a Mc MP5 color CCD camera for photograph collection.

Acknowledgements

This work was supported by the 973 Program (2011CB932502) and by the NSFC (nos. 20932004 and 21172119), which are gratefully acknowledged.

[1] a) D. Y. Chen, M. Jiang, *Acc. Chem. Res.* **2005**, *38*, 494–502; b) D. Y. Yan, Y. F. Zhou, *Science* **2004**, *303*, 65–67; c) P. Jonkheijm, E. W. Meijer, *Science* **2006**, *313*, 80–83.

[2] a) C. Wang, S. Yin, S. Chen, H. Xu, Z. Wang, X. Zhang, *Angew. Chem.* **2008**, *120*, 9189–9192; *Angew. Chem. Int. Ed.* **2008**, *47*, 9049–9052; b) C. Park, I. H. Lee, S. Lee, Y. Song, M. Rhue, C. Kim, *Proc. Natl. Acad. Sci. USA* **2006**, *103*, 1199–1203; c) X. Zhang, Z. Chen, F. Würthner, *J. Am. Chem. Soc.* **2007**, *129*, 4886–4887.

[3] a) G. K. Voeltz, T. A. Rapoport, *Cell* **2006**, *124*, 573–586; b) G. K. Voeltz, M. M. Rolls, T. A. Rapoport, *EMBO Rep.* **2002**, *3*, 944–950; c) Y. Liu, C.-F. Ke, H.-Y. Zhang, J. Cui, F. Ding, *J. Am. Chem. Soc.* **2008**, *130*, 600–605.

[4] a) J.-M. Lehn, *Angew. Chem.* **1990**, *102*, 1347–1362; *Angew. Chem. Int. Ed. Engl.* **1990**, *29*, 1304–1319; b) G. M. Whitesides, B. Grzybowski, *Science* **2002**, *295*, 2418–2421; c) K. Kinbara, T. Aida, *Chem. Rev.* **2005**, *105*, 1377–1400.

[5] a) D.-S. Guo, K. Wang, Y. Liu, *J. Inclusion Phenom. Macrocyclic Chem.* **2008**, *62*, 1–21; b) F. Perret, A. N. Lazar, A. W. Coleman, *Chem. Commun.* **2006**, 2425–2438; c) F. Perret, A. W. Coleman, *Chem. Commun.* **2011**, *47*, 7303–7319.

[6] J. Cui, V. D. Uzunova, D.-S. Guo, K. Wang, W. M. Nau, Y. Liu, *Eur. J. Org. Chem.* **2010**, 1704–1710.

[7] a) D.-S. Guo, K. Chen, H.-Q. Zhang, Y. Liu, *Chem. Asian J.* **2009**, *4*, 436–445; b) D.-S. Guo, S. Chen, H. Qian, H.-Q. Zhang, Y. Liu, *Chem. Commun.* **2010**, *46*, 2620–2622; c) K. Wang, D.-S. Guo, Y. Liu, *Chem. Eur. J.* **2010**, *16*, 8006–8011; d) K. Wang, D.-S. Guo, X. Wang, Y. Liu, *ACS Nano* **2011**, *5*, 2880–2894; e) V. Francisco, N. Basilio, L. García-Río, J. R. Leis, E. F. Maques, C. Vázquez-Vázquez, *Chem. Commun.* **2010**, *46*, 6551–6553.

[8] K. Kalyanasundaram, J. K. Thomas, *J. Am. Chem. Soc.* **1977**, *99*, 2039–2044.

[9] M. Rehm, M. Frank, J. Schatz, *Tetrahedron Lett.* **2009**, *50*, 93–96.

[10] M. Lee, S.-J. Lee, L.-H. Jiang, *J. Am. Chem. Soc.* **2004**, *126*, 12724–12725.

[11] L. D. C. Baldi, E. T. Iamazaki, T. D. Z. Atvars, *Dyes Pigm.* **2008**, *76*, 669–676.

[12] D.-S. Guo, X. Su, Y. Liu, *Cryst. Growth Des.* **2008**, *8*, 3514–3517.

[13] D.-S. Guo, L.-H. Wang, Y. Liu, *J. Org. Chem.* **2007**, *72*, 7775–7778.

[14] a) S. J. Dalgarno, J. L. Atwood, C. L. Raston, *Chem. Commun.* **2006**, 4567–4574; b) X. Su, D.-S. Guo, Y. Liu, *CrystEngComm* **2010**, *12*, 947–952; c) Y. Liu, D.-S. Guo, H.-Y. Zhang, F. Ding, K. Chen, H.-B. Song, *Chem. Eur. J.* **2007**, *13*, 466–472.

[15] a) X. Guo, F. C. Szoka, *Acc. Chem. Res.* **2003**, *36*, 335–341; b) J. Zhu, R. J. Munn, M. H. Nantz, *J. Am. Chem. Soc.* **2000**, *122*, 2645–2646; c) M. Johnsson, A. Wagenaar, J. B. F. N. Engberts, *J. Am. Chem. Soc.* **2003**, *125*, 757–760; d) F. Chécot, S. Lecommandoux, Y. Gnanou, H.-A. Klok, *Angew. Chem.* **2002**, *114*, 1395–1399; *Angew. Chem. Int. Ed.* **2002**, *41*, 1339–1343; e) Y. Sumida, A. Masuyama, M. Takasu, T. Kida, Y. Nakatsuji, I. Ikeda, M. Nojima, *Langmuir* **2001**, *17*, 609–612; f) D. C. Drummond, M. Zignani, J.-C. Leroux, *Prog. Lipid Res.* **2000**, *39*, 409–460.

[16] a) Z. Chen, A. Lohr, C. R. Saha-Möller, F. Würthner, *Chem. Soc. Rev.* **2009**, *38*, 564–584; b) Z. Chen, V. Stepanenko, V. Dehm, P. Prins, L. D. A. Siebbeles, J. Seibt, P. Marquetand, V. Engel, F. Würthner, *Chem. Eur. J.* **2007**, *13*, 436–449.

[17] G. Arena, A. Contino, G. G. Lombardo, D. Sciotto, *Thermochim. Acta* **1995**, *264*, 1–11.

[18] J. W. Steed, C. P. Johnson, C. L. Barnes, R. K. Juneja, J. L. Atwood, S. Reilly, R. L. Hollis, P. H. Smith, D. L. Clark, *J. Am. Chem. Soc.* **1995**, *117*, 11426–11433.

[19] S. Shinkai, S. Mori, H. Koreishi, T. Tsubaki, O. Manabe, *J. Am. Chem. Soc.* **1986**, *108*, 2409–2416.

Received: March 19, 2012
Published online: June 11, 2012

